analytical chemistry

pubs.acs.org/ac Article

Microfluidic-Integrated Chip Resonators for Electron Spin Sensing in Submicromolar, Submicroliter Solutions

Nandita Abhyankar,* Megan A. Catterton, Gregory A. Cooksey, and Veronika A. Szalai*

Cite This: https://doi.org/10.1021/acs.analchem.4c00464 Read Online

ACCESS | Metrics & More | Article Recommendations | Supporting Information

ABSTRACT: Planar or chip microresonators decrease the sample volume required for magnetic resonance spectroscopies to the nanoliter scale. However, the interrogation of nanoliter-scale solution samples on planar sensors is hindered by the lack of microfluidic devices that can simultaneously provide a small total volume and long-term sample stability. Here, we report microfluidic devices that decrease the total required sample volume to the submicroliter scale and also provide long-term physical stability and storability. We also report a 3D-printed microfluidic with a self-contained actuation mechanism, which allows the sample to be retracted from the microresonator surface for storage. The microfluidic devices are fabricated easily by laser cutting or 3D printing and are integrable with a broad range of planar sensors. We use planar inverse anapole (PIA) microresonators to obtain continuous wave (CW) electron paramagnetic resonance (EPR) spectra of natural-isotopic-abundance nitroxide radicals, which are ubiquitously used as reporters of biomolecular dynamics. We provide experimental evidence for a concentration sensitivity of 330 ± 40 nmol L^{-1}, a concentration sensitivity limit of 800 ± 100 nmol $L^{-1}/mT\sqrt{Hz}$, and an active volume no greater than 30 nL. Together, these developments represent an advance not only in the sensitivity of EPR spectroscopy but also in the design of microfluidics for stable, dead-volume-free placement of nanoliter-scale volumes of solutions on planar sensors.

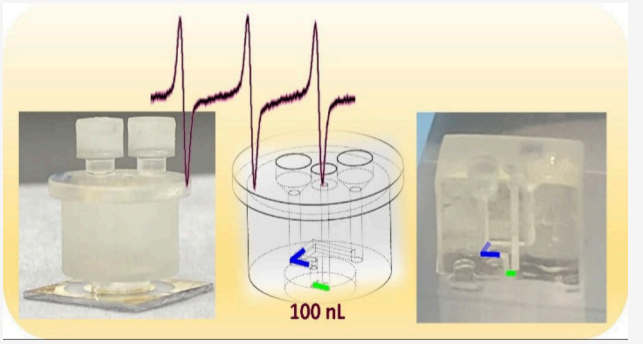

Magnetic resonance spectroscopies based on inductive detection are powerful and versatile techniques that provide atomic-level structural and functional information about a wide range of samples under broadly variable conditions. Spin detection in volume-limited samples has applications in many fields, spanning structural biology, quantum information processing, and solid-state physics.[1−5] The smaller wavelengths required for electron paramagnetic resonance (EPR) spectroscopy have enabled planar microresonators that can detect as few as 10^7 spins/$\sqrt{Hz}$ from subnanoliter volumes at room temperature.[2] Such low sensitivity limits make planar electron spin sensors desirable for a broad range of applications, e.g., biomacromolecular structure and dynamics, biosensing, and spin sensing close to the quantum regime. For solution-state samples, integration with microfluidic devices is required to lower the actual sample volume and exploit the low sensitivity limits provided by planar microcoils. Although EPR microresonators have been integrated with nanoliter- or microliter-scale microfluidics previously,[6,7] these previous integrated devices do not simultaneously provide the following capabilities required for broad applicability of planar microresonators in the full range of EPR measurements: (i) concentration sensitivity limits low enough to allow measurements without protein agglomeration (usually less than 200 μmol L^{-1}); (ii) the ability to conduct measurements and store samples for periods of several days or weeks; (iii) the ability to store and remeasure samples after long periods of time. Here, we report microfluidic devices that simultaneously provide these capabilities. We have integrated these microfluidic devices with planar inverse anapole (PIA) resonators, which have previously been shown to provide superior sensitivity in EPR measurements of solid-state samples.[8] We anticipate that the microfluidic devices reported here may be generally applied to any planar sensor for long-term, nondestructive measurements on nanoliter-scale samples of stable paramagnetic species.

The PIA microresonator is a planar spin sensor capable of detecting changes in transient magnetization of samples with subnanoliter volumes.[8] It confines the microwave magnetic field (B_1) to a nanoliter-scale mode volume at the center of the structure — we refer to this volume as the B_1 "hotspot". In the PIA design, radiative losses—arising from the electric dipole

Received: January 24, 2024
Revised: September 19, 2024
Accepted: September 19, 2024

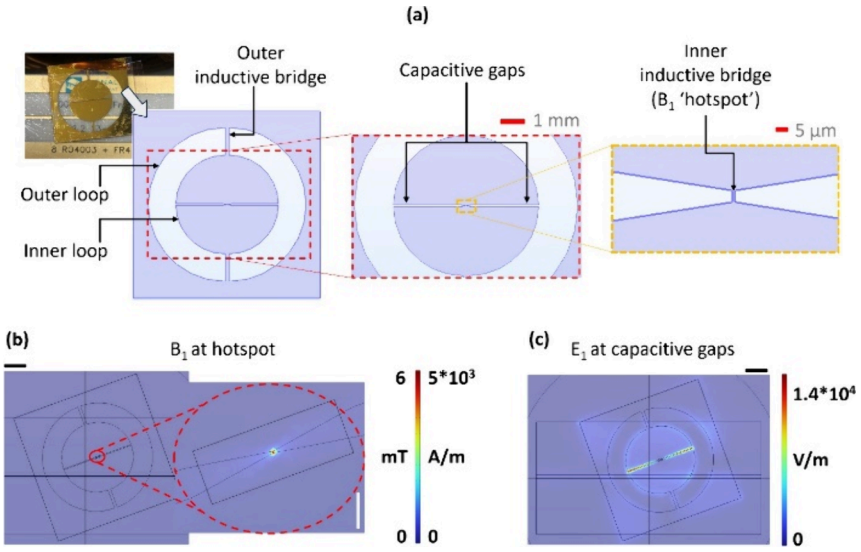

Figure 1. (a) The photograph on the top-left shows the PIA microresonator placed on the microstrip (which is the feedline for incident microwaves). The three panels from left to right show the top-view of the finite element model (FEM), i.e., simulation of the microresonator, with successively higher magnifications of the center of the device. The purple-shaded areas indicate the region on which gold is deposited to form the PIA microresonator, while the lighter region is the part of the dielectric substrate on which there is no gold. (b) FEM simulation of the microwave magnetic-field (B_1) distribution in the coupled microresonator-microstrip device, showing how B_1 is confined to a nanoliter-scale volume at the central metal bridge of the PIA microresonator. Horizontal black scale bar: 2 mm. Vertical white scale bar in the zoomed-in portion on the right: 100 μm. (c) FEM simulation of the microwave electric-field (E_1) distribution in the coupled microresonator-microstrip device. E_1 is concentrated over the capacitive gaps, with maxima on the outer edges. Horizontal black scale bar: 2 mm.

component (E_1) of the microwaves contained on the planar sensor—are reduced in comparison with other planar microresonators, thus improving quality-factor Q and consequently the sensitivity.

Even though microresonators reduce the sample volume required for measurement, they are difficult to apply for solution-state samples. The critical requirement of long-term physical stability of the sample is hindered in planar microresonators by the combination of small volumes and the fast rate of evaporation from surfaces. A further challenge is making sample placement reversible and repeatable. There are no reports of microfluidics that maintain solution volumes <100 nL on planar sensors for more than a few hours. In previous reports of EPR microresonators integrated with microfluidics,[6,7] either the total sample volume is not submicroliter or a submicroliter volume is not stable in the microfluidic for more than a few hours at room temperature. Designs of other microfluidics on other types of planar sensors require a large total sample volume in order to actuate the sample into a small active volume (e.g., by using a syringe pump).[9−14] In these designs, the minimum required sample volume is determined not by the active volume of the sensor but rather by the dead volume of the microfluidic channel, stemming from the volume of the interfacing channel and/or control reservoir.

Here, we report microfluidic devices with a total volume smaller than 100 nL, integrated with PIA microresonators, to enable EPR spectroscopy of solution-state biomacromolecular samples. We aim to create systems that are simple to use, integrate easily with spectrometers and other instruments, and consume minimal amounts of reagent. Because the smallest volume that can be dispensed by commercially available manual micropipettors is 100 nL, our first microfluidic design enables direct dispensation of this solution volume on the resonator surface. We demonstrate that samples are stable in this integrated microfluidic-microresonator device for several days of signal averaging and several weeks of storage at −80 °C. In our second microfluidic device, we have created a system that provides the sample storage and delivery capabilities of EPR spectroscopy with cavity resonators, where the sample solution is placed in a capillary tube that can be stored separately from the resonator. This second microfluidic design allows repeatable placement and removal of a sample from the resonator's active surface, followed by long-term storage for future use. To realize the second design, we used a widely accessible method of fabrication, namely, 3D printing, which enables inexpensive, easy, and scalable fabrication of 3D channels with volumes as small as 10 nL.[15] 3D printing has been used in innovative ways to make modular microfluidics and devices that eliminate off-chip equipment required to actuate small volumes.[16,17] The design reported in this work provides new capabilities for manipulating nanoliter-scale fluid volumes in multiple dimensions, thus providing facile loading and storage of small volumes in devices that can be separated from the planar resonator. Together, these developments represent an advance not only in the sensitivity of solution EPR spectroscopy but also in the design of microfluidics that reduce the total required sample volume to the order of 100 nL.

RESULTS AND DISCUSSION

Resonator Design. In the PIA architecture, a centimeter-scale outer loop structure (first two panels in Figure 1a) directs currents to a micron-scale wire or "hotspot" at the center of the resonator (right-most panel in Figure 1a); the microwave magnetic field B_1 is confined around this micron-scale wire, resulting in a nanoliter-scale magnetic mode volume confined to the center of the resonator (Figure 1b).[8] The microwave magnetic field is well-separated from the electric field E_1 (Figure 1c), eliminating losses arising from interactions with

https://doi.org/10.1021/acs.analchem.4c00464
Anal. Chem. XXXX, XXX, XXX−XXX

lossy dielectric samples. We have previously reported the PIA structure in detail in ref 14. The devices reported here were simulated by using the finite element method (FEM). The original PIA design employed a high-k, low-loss dielectric—lanthanum aluminate—strontium aluminum tantalate (LSAT).[8] Here, we replaced this expensive dielectric with a much cheaper alternative, quartz, which also provides the added advantage of a clean spectral background due to the lack of defects. We take advantage of the low loss-tangent of quartz and the flexibility of the PIA design to maintain the same Q factor and B_1 confinement despite the change of the dielectric substrate. The specific design parameters for the resonators used in the present report (Figure S1), discussion of the design rationale (Section S1), and a schematic of the fabrication process (Figure S2) are provided in the Supporting Information. Extensive details are in the Experimental Methods and Materials (Section S7 of the Supporting Information).

Microresonator-Microstrip Device Configuration. In EPR spectroscopy, the incident microwave propagates through a waveguide and is then weakly coupled to the spin-containing sample via the resonator.[18] In the present case, the waveguide is a 50 Ω-terminated microstrip, and the resonator is the PIA microresonator. The PIA microresonator is affixed to the microstrip using a small amount of silicone grease. One of the advantages of the PIA microresonator-microstrip device is that both tuning of device frequency and coupling between the microresonator and microstrip can be finely controlled through minor changes in the position of the microresonator relative to the central conductor of the microstrip (Figure 2a). We

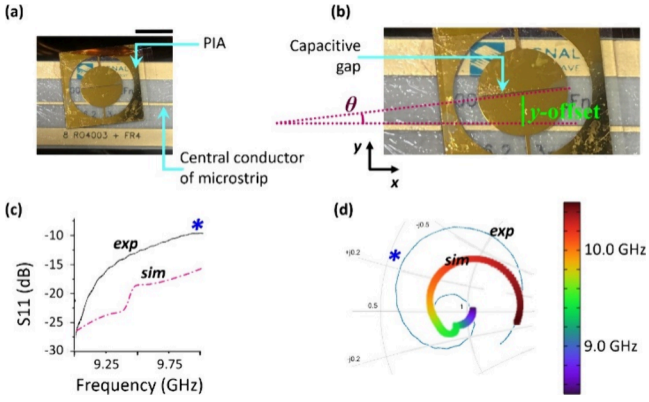

Figure 2. (a) Top view of a microresonator-microstrip device in the overcoupled state (see description in the adjoining text). Scale bar on top-right: 5 mm. (b) Magnified top-view of the microresonator-microstrip device, illustrated with the parameters θ and y-offset. (c) Comparison of experimental and simulated frequency profiles of the reflection coefficient (S11) for an overcoupled microresonator-microstrip device. (d) Comparison of experimental and simulated Smith charts that provide evidence of the overcoupled state. The blue asterisk on the experimental S11 profile and Smith chart indicates the measurement frequency of approximately 9.9 GHz.

describe the microresonator position using three parameters: x, y-offset, and θ (Figure 2b). The device is overcoupled at a measurement frequency of 9.9 GHz, as indicated by the S11-frequency profile (Figure 2c) and Smith chart (Figure 2d) of the microstrip-microresonator device. A brief explanation of the factors contributing to the EPR signal and noise is provided in Section S2 of the Supporting Information. An explanation of how to configure the overcoupled device and why an overcoupled device provides maximum sensitivity at a measurement frequency of 9.9 GHz is provided in Section S3 and Figure S3 of the Supporting Information.

Concentration Sensitivity. To test the concentration sensitivity of the quartz PIA microresonator, CW EPR spectra were obtained from submicroliter solution volumes localized at the B_1 hotspot, with the microresonator-microstrip device configured in the overcoupled state as described in the preceding section. For solution placement, a hole with a diameter of 1.0 ± 0.2 mm was created by laser-cutting through a quartz slide with a thickness of 1.00 ± 0.01 mm, resulting in a total volume of 800 ± 300 nL. This cut piece of quartz was adhered to the PIA microresonator using epoxy adhesive, with the hole centered on the hotspot, creating a microwell that could then be filled to localize submicroliter volumes of solution on the microresonator surface (first two panels in Figure 3a). A manual micropipettor was used to dispense

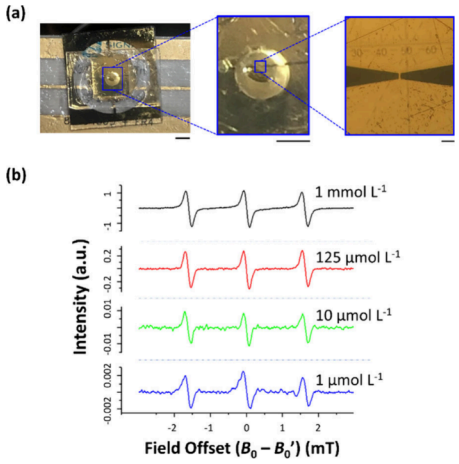

Figure 3. (a) Top view of the microresonator with a quartz microwell positioned over the microresonator hotspot. The sample is added to the microwell and the top is sealed off with a quartz coverslip adhered using silicone grease. Scale bar on the bottom right: 2 mm. The middle and right-most panels show successively higher magnifications of the central active region of the PIA microresonator. The middle panel shows the top view of the microwell placed on the active region. Scale bar: 1 mm. The right-most micrograph shows the 1 μm × 5 μm inductive bridge that produces the active region of the microresonator. Scale bar: 10 μm. (b) Continuous wave (CW) EPR spectra obtained for a series of solutions of the 3-Carboxy-proxyl radical (*aq.*) with concentrations ranging from 1 mmol L^{-1} to 1 μmol L^{-1}. Spectra are plotted as a function of the B_0-field offset, $B_0'-B_0$; here, B_0 is the center field of the central peak of the hyperfine triplet. Thus, all spectra are centered at $B_0'-B_0 = 0$ mT. Figure S4 in the Supporting Information shows an overlay of spectra for 1 mmol L^{-1} and 1 μmol L^{-1}, which are identical in all respects except for absolute signal intensity and signal-to-noise ratio.

approximately 200 to 500 nL of solution into the microwell described above. This large volume, which is more than two orders of magnitude higher than the active volume (as demonstrated in the next section), was used deliberately to ensure that signal changes arose solely from a change in spin concentration and not from variations in sample volume. Placement of solution on the resonator hotspot (shown in the last panel of Figure 3a) did not impact the coupling or frequency profile of the device. This observation indicates that the lossy dielectric water does not interact with E_1, consistent with simulations showing that the E_1 maxima in the PIA design

https://doi.org/10.1021/acs.analchem.4c00464
Anal. Chem. XXXX, XXX, XXX−XXX

Table 1. Comparison of Performance Parameters of the Integrated PIA-Microfluidic Device and Those of Previously Reported Integrated Microresonator-Microfluidic Devices for EPR Spectroscopy

integrated device	ParPar[6]	double split-ring[7]	planar inverse anapole (this report)
microresonator description and mode volume	ParPar resonators (TiAu layers on Si substrate) with calculated mode volumes of 1 nL to 3.6 nL	double split-ring resonator (copper on polyimide); mode volume ≈ 1 μL	planar inverse anapole resonator (TiAu/CrAu on silica substrate), with a calculated mode volume of approximately 3 nL
microfluidic description	channels etched in freestanding AAO wafers	channels made by laser-cutting of polyimide sheets	channels or microwells made by laser-cutting of quartz slides or by 3D printing
volume of microfluidic channel	30 nL	2 μL	30 nL
reported concentration sensitivity limit for a nitroxide radical at room temperature (μmol $L^{-1}/\sqrt{mT}$ Hz)	7.8	8.5	0.8 ± 0.1
reported stability of sample against evaporation	reported up to 6 h	undefined	47 days stored at −80 °C, stable for room-temperature measurements of several days
ability to retract and store sample	no	no	yes

are spatially well-separated from the B_1 maximum. Figure 3b shows CW EPR spectra for a series of solutions of the 3-Carboxy-proxyl radical in water, with concentrations in the range of approximately 1 mmol L^{-1} to 1 μmol L^{-1}. All spectra were collected at a frequency of 9.87 ± 0.02 GHz; the uncertainty in measurement frequency in this set of spectra stems from slight variations in y-offset and θ because of manual positioning of the resonator to obtain the coupled microresonator-microstrip device. The spectra are acquired in the frequency-locked mode; i.e., there is negligible frequency drift after a device is configured and the frequency is locked to a particular value. The observed frequency drift during measurement is ±0.0001 GHz, comparable to that obtained when the spectrometer is operated in the conventional manner using automatic frequency control (AFC) during collection of CW EPR spectra. In our case, the measurement frequency is locked and the signal phase is then adjusted to obtain the first-derivative line shape typical of CW EPR spectra.

A comparison of the performance of our design with previously reported microresonator-microfluidic EPR devices is provided in Table 1. We have demonstrated the acquisition of the CW EPR spectrum of a solution with a concentration of 1 ± 0.1 μmol L^{-1}, i.e. a concentration of 330 ± 40 nmol L^{-1} per hyperfine line, leading to a concentration sensitivity limit of 800 ± 100 nmol $L^{-1}/mT\sqrt{Hz}$. The complete calculation of the concentration sensitivity limit is given in Section S4 of the Supporting Information. Measurement parameters and spectral line widths are provided in Table S1 of the Supporting Information. These results demonstrate that we have achieved submicromolar concentration sensitivity with essentially "disposable" PIA microresonators fabricated on quartz, an inexpensive low-k, low-loss substrate. Our concentration sensitivity limit is improved by an order of magnitude compared to previous reports, while maintaining a sample volume smaller than 100 nL.

We note here that optically detected magnetic resonance of just a few spins confined in zeptoliter volumes around the NV center in a diamond is possible.[19,20] However, it is yet to be proven that these methodologies may be applied to a wide range of samples, including solutions of peptides labeled with nitroxide radicals, as are routinely used in biomolecular EPR studies. Inductive detection is still the predominant modality of EPR spectroscopy due to its broad applicability and superior spectroscopic capabilities.

Microfluidic Design and Volume Sensitivity. With the aforementioned goals of minimizing sample volume and maximizing physical stability of the sample in the microfluidic channel, we designed two types of microfluidic devices; in both cases, we loaded the microfluidic device using commercially available manual micropipettors that can dispense a minimum volume of 100 nL. In the first iteration, we designed a microfluidic device to hold a solution volume up to 100 nL on the microresonator surface for several days. In this design, once the microresonator is placed on the solution, it cannot be retrieved and stored separately for future use. However, in the typical practice of EPR spectroscopy of solution samples, multiple samples are measured in succession using the same resonator, and samples are stored and remeasured several times. This capability was achieved with our second iteration of the microfluidic device realized by using 3D printing. The 3D-printed microfluidic requires a larger total volume but provides the capability for repeatable sample dispensation and retrieval from the microresonator surface (for example, for repeated measurements of the same sample or measurements of several different samples on the same resonator). We describe both microfluidic designs below.

Figure 4a shows our two-layer quartz microfluidic device, in which each layer was made by laser-cutting through quartz coverslips (details in Experimental Materials and Methods, Section S7 of the Supporting Information). Using a micropipettor, a solution volume of approximately 100 nL was dispensed into the inlet port of Layer 2, which then filled the sample well in Layer 1 by capillary action. The outlet port of the top layer (Layer 2) allows the solution to move through the channel by displacing air. After sample dispensation, the top layer with inlet and outlet ports was sealed by using a single piece of quartz coated with silicone grease. The thickness of the quartz coverslip was 0.150 ± 0.005 mm; the length l of the sample well in contact with the microresonator was 1.0 ± 0.1 mm. A sample well with a width w of 0.20 ± 0.05 mm resulted in a sample-well volume of 30 ± 3 nL. Increasing w to 0.60 ± 0.05 mm produced a sample-well volume of approximately 90 ± 3 nL. These sample wells of differing volumes can be used to demonstrate a lower experimental limit for the active volume. For example, here we show that the active volume of the resonator is at most 30 nL because increasing the sample volume to 90 nL does not increase the signal intensity appreciably. Figure 4b shows a comparison of the EPR spectra of a solution of 3-Carboxy-proxyl (*aq.*) at a concentration of 1 mmol L^{-1} in the 30 nL and 90 nL wells. The same spectra are plotted as a function of the g-factor in Figure S5 (30 nL) and Figure S6 (90 nL) of the Supporting Information and show that the precision in g-factor after manual repositioning for different samples is ±0.0001. The sample in the smaller sample well yielded a double-integrated (DI) signal intensity of 14.6 ± 0.2 a.u. Increasing the sample

https://doi.org/10.1021/acs.analchem.4c00464
Anal. Chem. XXXX, XXX, XXX−XXX

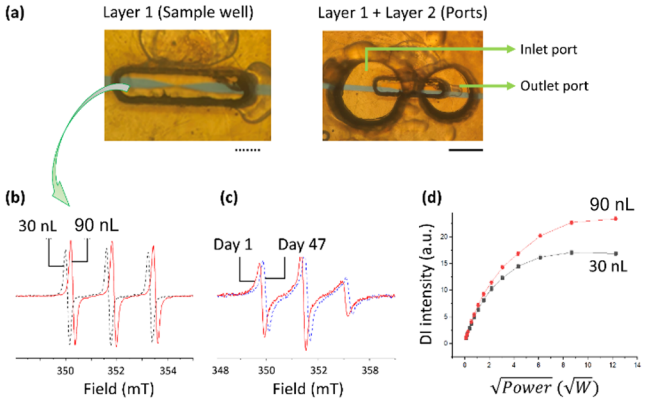

Figure 4. (a) Micrographs of the two-layer quartz microfluidic device at the assembly stage for each layer. In these images, the sample well in Layer 1 has a length, *l*, of 1.0 ± 0.1 mm, width, *w*, of 0.20 ± 0.05 mm, and thickness (perpendicular to the plane of the micrograph) of 0.150 ± 0.002 mm. After assembly, a solution volume of approximately 100 nL is dispensed into the inlet port using a micropipettor. Scale bar on bottom right: 1 mm. (b) Comparison of EPR spectra of a 1 mmol L^{-1} solution of 3-Carboxy-proxyl (*aq.*) acquired in sample wells with volumes of 30 nL (dashed line) or 90 nL (solid line). The acquisition frequency for the black dashed spectrum was 9.8692 ± 0.0002 GHz, while that for the solid red spectrum was 9.8756 ± 0.0002 GHz, where the frequency uncertainty represents the frequency drift while the spectrometer is operating in frequency-locked mode. (c) Comparison of EPR spectra of a spin-labeled protein before (solid line) and after (dashed line) long-term storage at −80 °C. The acquisition frequency for the solid red spectrum was 9.8630 ± 0.0002 GHz, while that for the blue dashed spectrum was 9.8668 ± 0.0002 GHz. (d) Power saturation curves for solution in a 30 nL well (circles) or a 90 nL well (squares). The error bars are smaller than or equal to the data point size.

size to 90 nL resulted in a DI signal intensity of 17.0 ± 0.3 a.u. (uncertainties in DI intensity represent the standard deviation of three measurements). Thus, even though the sample volume was increased by 300%, the DI signal intensity only increased by approximately 14 ± 2 % − indicating that 30 nL provides more than 86 ± 2% of the signal intensity. We have thus demonstrated experimentally that the active volume of the quartz PIA microresonator is *at most* 30 nL.

To test the stability of this microfluidic device and its consequent utility for analyzing spin-labeled biomacromolecular samples, a microresonator-microfluidic chip was filled with a spin-labeled protein, and CW EPR spectra were collected. The chip was then stored at −80 °C for an extended time (47 days in this case), after which it was removed from the freezer and thawed under ambient conditions. The microfluidic-microresonator chip was again adhered to the microstrip by using a small amount of silicone grease. The microresonator-microstrip device was reconfigured in the overcoupled state, and EPR spectra were acquired under the same conditions used previously. Comparison of the spectra acquired before and after long-term storage (Figure 4c) shows that the solution was stably contained in the microfluidic and that the microfluidic-microresonator chip survived freezing and thawing without formation of leaks. The same spectra are plotted as a function of the g-factor in Figure S6 of the Supporting Information and show that the precision in g-factor after manual repositioning for different samples is ±0.0001. Lastly, the power dependence of signal intensity for a given sample shape can also be used to indirectly probe the B_1 distribution around the resonator hotspot. A comparison of saturation curves (Figure 4d) for the solution in the 30 and 90 nL wells shows that when the signals are power-saturated, the larger volume provides a larger gain in signal. This behavior is consistent with the inhomogeneous B_1-distribution characteristic of planar microresonators (Figure S7 in the Supporting Information). We surmise that the additional sensitivity obtained at higher powers from the larger sample is provided by peripheral low-B_1 regions of the active volume that are not yet power-saturated. The power-to-field conversion efficiency for the overcoupled device was found to be (2.5 ± 0.5) mT/$\sqrt{W}$ (obtained from the saturation curve for microcrystalline BDPA, Figure S8 in the Supporting Information).

As mentioned previously, the second type of microfluidic device was designed to address the more challenging requirement of repeatable sample dispensation and retrieval of volumes smaller than 100 nL from the microresonator surface. To achieve this functionality, we have developed a self-contained microfluidic with an actuation mechanism that enables reversible motion of fluid samples in a monolithic, 3D structure affixed on the microresonator surface. In this device, the sample initialization/storage position is in the interior of the button-shaped microfluidic, away from the microresonator surface. From this position, a smaller fraction of the sample can be pushed to the measurement position using a plunger inserted in the sample port. The measurement position is in a sample channel that is adhered to the microresonator surface to form the sample well. The total volume from the sample port to the initialization point is designed to be approximately 2 μL while the volume of the sample well is designed to be 60 nL in the device reported here. When the measurement is completed, the sample can be retracted back into the storage position, and the microfluidic device can be separated from the microresonator surface to be stored separately. Figure 5a shows the schematic of this monolithic 3D-printed device. Figure 5b shows a photograph of the microfluidic device adhered on the resonator surface; a dimensioned drawing is provided in Figure S9 of the Supporting Information. Figure 5c shows a schematic of how the sample can be separated from the resonator surface and stored for subsequent measurements at later times. A detailed description of the device operation is provided in Section S5 of the Supporting Information. Additionally, for direct demonstration, we have fabricated a device with flat and transparent walls, which allow a view of the sample and silicone oil moving in the interior of the device. A video of the device operation (S12_Device_Operation) is provided in the Supporting Information. A comparison of the device and the computer-aided drawing is also provided in Figure S10 of the Supporting Information.

The functionality of the microfluidic device is evidenced by a comparison of the spectra obtained for consecutive dispensations of a 1 mmol L^{-1} aqueous solution of the 3-Carboxy-proxyl radical (Figure 5d). No signal intensity is lost in consecutive dispensations. The same spectra are plotted as a function of the g-factor in Figure S11 of the Supporting Information. The slightly larger volume of 60 nL for the sample well was designed to facilitate the positioning of the device on the microresonator. The surface of the microresonator and the interior surface of the microfluidic can both be treated to minimize interaction with the sample in a manner customized to the specific experiment or sample being studied. In the case presented here, the resonator surface is coated with silicon nitride to protect the soft gold layer from abrasion.

https://doi.org/10.1021/acs.analchem.4c00464
Anal. Chem. XXXX, XXX, XXX−XXX

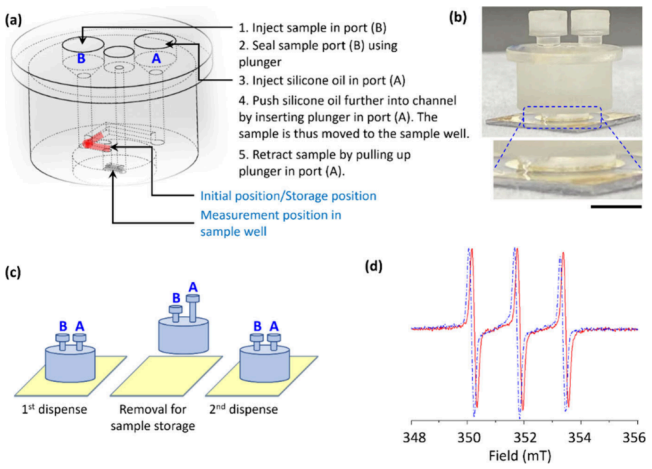

Figure 5. (a) Computer-aided design of the 3D-printed microfluidic device that allows dispensation, retraction, and subsequent removal of a solution from the microresonator surface. The procedure for filling the device and moving the solution to the sample well is delineated. The red region indicates the sample when it is initially placed at the bottom of the sample port. The gray region indicates the sample well, where the sample is located during measurements. (b) Photograph of the 3D-printed microfluidic device with plungers placed in ports; the microfluidic device is adhered to the microresonator surface using silicone glue. The zoomed region in the blue dashed box shows the narrow bottom part of the microfluidic adhered to the microresonator (explanation in text above). Scale bar: 5 mm. (c) Schematic of sample dispensation from microfluidic adhered to microresonator surface, sample retraction and separation of microfluidic device, and sample redispensation after readhering microfluidic to resonator surface. (d) Comparison of spectra obtained from the first and second dispensations. The red solid line spectrum was acquired at 9.8748 ± 0.0002 GHz while the blue dashed line spectrum was acquired at 9.8718 ± 0.0002 GHz. The frequency uncertainty arises from frequency drift while the spectrometer is operating in frequency-locked mode.

Silicon nitride can be treated to make it hydrophilic or hydrophobic, as required to minimize the interaction with the desired sample.

Pulse EPR. Pulse EPR measurements such as electron spin echo envelope modulation (ESEEM), hyperfine sublevel correlation spectroscopy (HYSCORE), and double-electron electron resonance (DEER *aka* PELDOR) provide valuable information about the structure and dynamics of biological systems. These measurements are typically conducted at temperatures below 80 K, which is out of the scope of the present report. However, pulse measurements on a solid sample at room temperature can provide an idea of the pulse capability of the PIA microresonators reported here. We conducted demonstrative pulse experiments on a solid sample of BDPA-doped PMMA. The echo-detected field sweeps reproduced the line width of (8 ± 0.2) G obtained from CW EPR spectra of the inhomogeneously doped BDPA:PMMA sample. We also obtained nutation curves, in which the first minimum was prominent followed by rapidly decaying subsequent minima, as is typical for planar microresonators because of B_1-inhomogeneity.[6] The results of pulse experiments are plotted in Figure S12 and discussed further in Section S6 of the Supporting Information.

CONCLUSIONS

We have developed chip-integrated microfluidic devices with zero dead volume and the ability to actuate nanoliter-scale volumes in three dimensions. These microfluidic devices are potentially applicable to a broad range of planar sensors for solution measurements. The integrated microresonator-microfluidic devices reported here allow coupling of microwaves to spin ensembles in solution volumes as small as 30 nL. The microfluidic devices are made by either laser-cutting or 3D-printing and thus are easily fabricated in wet-lab or benchtop settings. We have demonstrated CW EPR spectroscopy of spin-labeled protein solutions with volumes smaller than 100 nL and at spin label concentrations as small as 330 ± 40 nmol L^{-1}. The microfluidic-integrated chips retain the same long-term stability and storability as capillary tubes typically used with cavity resonators, making this technology competitive with standard EPR spectroscopic resonators while reducing the required sample volume by 2 orders of magnitude. Moreover, we have developed 3D-printed microfluidics that can be used to dispense and retract nanoliter-scale volumes from planar surfaces, allowing long-term storage within the microfluidic device even when it is separated from the sensor.

EXPERIMENTAL METHODS AND MATERIALS

Details of methods and materials used in all experiments are provided in Section S7 of the Supporting Information.

ASSOCIATED CONTENT

Supporting Information

The Supporting Information is available free of charge at https://pubs.acs.org/doi/10.1021/acs.analchem.4c00464.

Design parameters for the PIA resonator; fabrication process for PIA microresonators; discussion of signal-to-noise ratio and explanation of overcoupled device; direct comparisons of EPR spectra from Figures 2, 3, 4, and 5; dimensioned drawing of the 3D-printed microresonator (PDF)

Video demonstration of the operation of the 3D-printed microresonator (MP4)

AUTHOR INFORMATION

Corresponding Authors

Nandita Abhyankar − *Institute for Research in Electronics and Applied Physics, University of Maryland, College Park, Maryland 20742, United States; National Institute of Standards and Technology, Gaithersburg, Maryland 20899, United States;* orcid.org/0000-0002-1991-2160; Email: nabhyank@umd.edu

Veronika A. Szalai − *National Institute of Standards and Technology, Gaithersburg, Maryland 20899, United States;* orcid.org/0000-0002-1115-2849; Email: veronika.szalai@nist.gov

Authors

Megan A. Catterton − *Department of Mechanical Engineering, Johns Hopkins University, Baltimore, Maryland 21218, United States; National Institute of Standards and Technology, Gaithersburg, Maryland 20899, United States*

Gregory A. Cooksey − *National Institute of Standards and Technology, Gaithersburg, Maryland 20899, United States;* orcid.org/0000-0003-0200-2715

Complete contact information is available at:

https://doi.org/10.1021/acs.analchem.4c00464
Anal. Chem. XXXX, XXX, XXX−XXX

https://pubs.acs.org/10.1021/acs.analchem.4c00464

Author Contributions

The manuscript was written through contributions of all authors. All authors have given approval to the final version of the manuscript.

Funding

N.A. acknowledges partial support from NIGMS Grant Award R21GM134406 and NIST MSE Award 70NANB21H183, both through the University of Maryland. M.C. acknowledges support from the Professional Research Experience Program at Johns Hopkins University and a fellowship from the National Research Council Research Associateship Program.

Notes

Certain commercial entities, equipment or materials may be identified in this document to describe an experimental procedure or concept adequately. Such identification is not intended to imply recommendation or endorsement by the National Institute of Standards and Technology, nor is it intended to imply that the entities, materials, or equipment are necessarily the best available for the purpose.

The authors declare no competing financial interest.

■ ACKNOWLEDGMENTS

Phyllis Robinson is acknowledged for providing the motivation for this work, which is to enable EPR spectroscopy of membrane proteins at sample volumes on the order of 100 nL. Rachel Kearns (UMD) & Zvi Kelman (NIST) are acknowledged for the cysteine variant of protein A used for spin-labeling. Portions of this work were conducted at the NIST Center for Nanoscale Science and Technology and in the Biomolecular Labeling Laboratory at the Institute for Bioscience & Biotechnology Research (IBBR).

■ ABBREVIATIONS

BDPA, 1,3-bisdiphenylene-2-phenylallyl; CAD, computer aided design; CC, central conductor; CW, continuous wave; dB, decibel; DI, double-integral; EDFS, echo-detected field sweep; EPR, electron paramagnetic resonance; ESEEM, electron spine-echo envelope modulation; FEM, finite element simulations; HYSCORE, hyperfine sublevel correlation spectroscopy; DEER, double-electron electron resonance; LSAT, lanthanum aluminate−strontium aluminum tantalate; MTSL, *S*-(1-oxyl-2,2,5,5-tetramethyl-2,5-dihydro-1H-pyrrol-3-yl)-methylmethanesulfonothioate; PIA, planar inverse anapole; PMMA, poly(methyl methacrylate); SNR, signal-to-noise ratio; SI, Supporting Information; UV, ultraviolet

■ REFERENCES

(1) Zalesskiy, S. S.; Danieli, E.; Blümich, B.; Ananikov, V. P. *Chem. Rev.* **2014**, *114* (11), 5641−5694.
(2) Abhyankar, N.; Agrawal, A.; Campbell, J.; Maly, T.; Shrestha, P.; Szalai, V. *Rev. Sci. Instrum.* **2022**, *93* (10), No. 101101.
(3) Yang, Q.; Zhao, J.; Dreyer, F.; Krüger, D.; Chu, A.; Kern, M.; Blümich, B.; Anders, J. *J. Magn. Reson.* **2024**, *358*, No. 107603.
(4) Kiss, S. Z.; MacKinnon, N.; Korvink, J. G. *Sci. Rep* **2021**, *11* (1), 4671.
(5) Morton, J. J. L.; Bertet, P. *J. Magn. Reson.* **2018**, *287*, 128−139.
(6) Dayan, N.; Ishay, Y.; Artzi, Y.; Cristea, D.; Driesschaert, B.; Blank, A. *Journal of Magnetic Resonance Open* **2020**, *2*−*3*, 100005.
(7) Kiss, S. Z.; Rostas, A. M.; Heidinger, L.; Spengler, N.; Meissner, M. V.; MacKinnon, N.; Schleicher, E.; Weber, S.; Korvink, J. G. *J. Magn. Reson.* **2016**, *270*, 169−175.
(8) Abhyankar, N.; Agrawal, A.; Shrestha, P.; Maier, R.; McMichael, R. D.; Campbell, J.; Szalai, V. *Sci. Adv.* **2020**, *6* (44), No. eabb0620.
(9) Werdich, A. A.; Lima, E. A.; Ivanov, B.; Ges, I.; Anderson, M. E.; Wikswo, J. P.; Baudenbacher, F. J. *Lab Chip* **2004**, *4* (4), 357.
(10) Bao, X.; Ocket, I.; Crupi, G.; Schreurs, D.; Bao, J.; Kil, D.; Puers, B.; Nauwelaers, B. *IEEE J. Electromagn. RF Microw. Med. Biol.* **2018**, *2* (1), 10−17.
(11) Abbasi, Z.; Baghelani, M.; Daneshmand, M. Disposable Microwave Sensor for Real-Time Monitoring and Content Sensing of Droplets in Microfluidic Devices. In *2020 IEEE International Symposium on Antennas and Propagation and North American Radio Science Meeting*; IEEE: Montreal, QC, Canada, 2020; pp 823−824. DOI: 10.1109/IEEECONF35879.2020.9329971.
(12) Kilpijärvi, J.; Halonen, N.; Juuti, J.; Hannu, J. *Sensors* **2019**, *19* (4), 819.
(13) Kratz, C.; Furchner, A.; Oates, T. W. H.; Janasek, D.; Hinrichs, K. *ACS Sens* **2018**, *3* (2), 299−303.
(14) Baghelani, M.; Abbasi, Z.; Daneshmand, M.; Light, P. E. *Sci. Rep* **2020**, *10* (1), No. 12980.
(15) Hinnen, H.; Viglione, M.; Munro, T. R.; Woolley, A. T.; Nordin, G. P. *Micromachines* **2023**, *14* (7), 1286.
(16) Bhargava, K. C.; Thompson, B.; Malmstadt, N. *Proc. Natl. Acad. Sci. U.S.A.* **2014**, *111* (42), 15013−15018.
(17) Chan, H. N.; Shu, Y.; Xiong, B.; Chen, Y.; Chen, Y.; Tian, Q.; Michael, S. A.; Shen, B.; Wu, H. *ACS Sens.* **2016**, *1* (3), 227−234.
(18) Elschner, B.; Poole, Ch. P. *Berichte der Bunsengesellschaft für physikalische Chemie* **1983**, *87* (12), 1230−1230.
(19) Shi, F.; Zhang, Q.; Wang, P.; Sun, H.; Wang, J.; Rong, X.; Chen, M.; Ju, C.; Reinhard, F.; Chen, H.; Wrachtrup, J.; Wang, J.; Du, J. *Science* **2015**, *347* (6226), 1135−1138.
(20) Kong, F.; Zhao, P.; Ye, X.; Wang, Z.; Qin, Z.; Yu, P.; Su, J.; Shi, F.; Du, J. *Nat. Commun.* **2018**, *9* (1), 1563.